Translational Oncology 36 (2023) 101741

Contents lists available at ScienceDirect

Translational Oncology

journal homepage: www.elsevier.com/locate/tranon

Identification of a novel 5-methylcytosine-related signature for prognostic prediction of kidney renal papillary cell carcinoma and a Putative target for drug repurposing

Zhen Zhang [a,*,1], Chuanhua Cao [b,c,1], Chun-Li Zhou [d], Xilong Li [a], Changhong Miao [e], Li Shen [f], Rajeev K. Singla [g,h,**], Xihua Lu [a,*]

[a] Department of Anesthesiology, The Affiliated Cancer Hospital of Zhengzhou University & Henan Cancer Hospital, Zhengzhou 450008, China
[b] Department of Oncology, Xiangyang Central Hospital, Affiliated Hospital of Hubei University of Arts and Science, Xiangyang 441021, China
[c] Institute of Oncology, Hubei University of Arts and Science, Xiangyang 441021, China
[d] Department of Anesthesiology, Xiangyang Central Hospital, Affiliated Hospital of Hubei University of Arts and Science, Xiangyang 441021, China
[e] Department of Anesthesiology, Cancer Hospital of Fudan University, Shanghai 200032, China
[f] Department of Biomedical Engineering, Hong Kong Polytechnic University, Hong Kong SAR, China
[g] Joint Laboratory of Artificial Intelligence for Critical Care Medicine, Department of Critical Care Medicine and Institutes for Systems Genetics, Frontiers Science Center for Disease-related Molecular Network, West China Hospital, Sichuan University, Chengdu, China
[h] School of Pharmaceutical Sciences, Lovely Professional University, Phagwara, Punjab-144411, India

ARTICLE INFO

Keywords:
Kidney renal papillary cell carcinoma
5-methylcytosine
Prognostic signature
Tumor microenvironment
Tumor therapy
Kidney cancer
Renal cell carcinoma

ABSTRACT

Background: Many studies have demonstrated the crucial roles of 5-methylcytosine (m5C) RNA methylation in cancer pathogenesis.
Methods: Two datasets, including TCGA-KIRP and ICGC, and related clinical information were downloaded, where the expression of 13 m5C regulators was examined. We applied LASSO regression to construct a multi-m5C-regulator-based signature in the TCGA cohort, which was further validated using the ICGC cohort. Univariate and multivariate Cox regressions were applied to evaluate the independent prognostic value of our model. The differences in biological functions and immune characterizations between high and low-risk groups divided based on the risk scores were also investigated via multiple approaches, such as enrichment analyses, mutation mining, and immune scoring. Finally, the sensitivities of commonly used targeted drugs were tested, and the connectivity MAP (cMAP) was utilized to screen potentially effective molecules for patients in the high-risk group. Experimental validation was done following qPCR tests in Caki-2 and HK-2 cell lines.
Results: 3 m5C regulators, including ALYREF, DNMT3B and YBX1, were involved in our model. Survival analysis revealed a worse prognosis for patients in the high-risk group. Cox regression results indicated our model's superior predictive performance compared to single-factor prognostic evaluation. Functional enrichment analyses indicated a higher mutation frequency and poorer tumor microenvironment of patients in the high-risk group. qPCR-based results revealed that ALYREF, DNMT3B, and YBX1 were significantly up-regulated in Caki-2 cell lines compared with HK-2 cell lines. Molecules like BRD-K72451865, Levosimendan, and BRD-K03515135 were advised by cMAP for patients in the high-risk group.
Conclusion: Our study presented a novel predictive model for KIRP prognosis. Furthermore, the results of our analysis provide new insights for investigating m5C events in KIRP pathogenesis.

* Corresponding authors.
** Corresponding author at: Department of Anesthesiology, The Affiliated Cancer Hospital of Zhengzhou University & Henan Cancer Hospital, Zhengzhou 450008, China and Joint Laboratory of Artificial Intelligence for Critical Care Medicine, Department of Critical Care Medicine and Institutes for Systems Genetics, Frontiers Science Center for Disease-related Molecular Network, West China Hospital, Sichuan University, Chengdu, China.
E-mail addresses: zlyyzhangzhen2130@zzu.edu.cn (Z. Zhang), rajeevsingla26@gmail.com (R.K. Singla), zlyyluxihua0258@zzu.edu.cn (X. Lu).
[1] These authors contributed equally to this work.

https://doi.org/10.1016/j.tranon.2023.101741
Received 26 July 2022; Received in revised form 14 March 2023; Accepted 17 July 2023
Available online 29 July 2023

Introduction

Renal cell carcinoma (RCC) is one of the most common tumors in the genitourinary system, accounting for about 3.7% of all malignant types of cancer worldwide [1]. The three main subtypes of RCC are clear cell renal cell carcinoma (ccRCC), kidney renal papillary cell carcinoma (KIRP), and chromophobe renal carcinoma (CRC). Although KIRP has less invasiveness and better prognostic performance compared with ccRCC, it is reported that around 25–35% of patients had distant metastasis in their initial diagnosis. Moreover, previous studies have shown that KIRP patients tend to have worse survival outcomes than ccRCC patients after metastases [2], and the 5-year survival rate of those patients is barely around 12% [3,4]. Therefore, a robust, accurate, and efficient clinical model is highly demanded to predict and evaluate patients' prognoses and identify potentially high-risk individuals. This may not only allow early intervention towards post-metastatic patients, but clinicians can also medicate patients at different risk levels more precisely and improve survival outcomes.

Methylation is a vital process in RNA post-transcriptional modification, which controls translation efficiency [5,6]. Accumulating pieces of evidence have revealed the significant roles of N6-methyladenosine (m6A) in epitranscriptional regulation [6] following studies that further determined its vast potential as a biomarker in the early detection of cancer [7,8]. Due to its promising clinical applications, efforts have been made to develop targeted methods and algorithms for the fast detection of such biomarkers [9–11]. Besides m6A, 5-methylcytosine (m5C) is another essential RNA modification process where the methyl group is bound to the fifth position of the cytosine ring catalyzed by RNA methyltransferase, which has drawn increasing attention in recent years. The prominent roles of m5C include stabilization of RNA structure, regulation of RNA metabolism, recognition of tRNA, and so on [6].

Meanwhile, investigations also disclosed its close association with cancer pathogeneses and development. For example, Chen et al. noticed that m5C might stabilize the mRNA expression via the regulation of YBX1 in bladder cancer, which further influences cancer cell proliferation and metastasis [12]. Furthermore, FMRP, a novel reader of m5C, can promote transcription-coupled homologous recombination and enhance the viability of cancer cells [13]. In addition, the signatures constructed based on m5C-related genes have shown their superior performances in the prediction and evaluation of cancer prognosis for lung adenocarcinoma [14], clear cell renal cell carcinoma [15], hepatocellular carcinoma [16], as well as breast cancer [17].

The rapid development of cancer immunotherapy has driven the field of RCC treatment into a new era. Immune Checkpoint Inhibitors (ICIs) targeting PD-1/PD-L1 and CTLA-4 have shown their remarkable

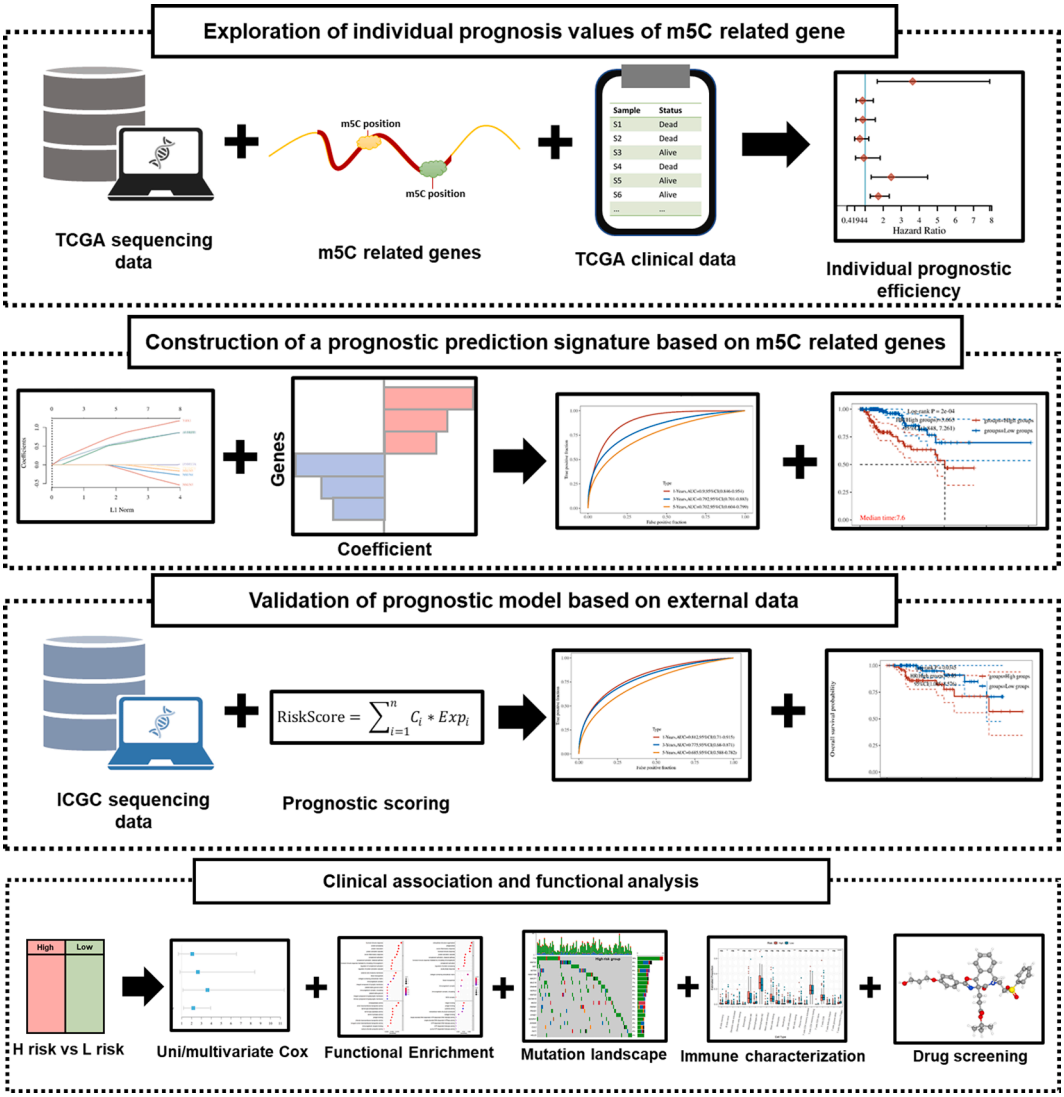

Fig. 1. The pipeline for this study.

Table 1
The clinical characteristics of KIRP patients in TCGA and ICGC.

	TCGA		ICGC	
Variables	No. of patients	Percentage (%)	No. of patients	Percentage (%)
Age (years)				
≥60	169	58.7	80	58.8
<60	119	41.3	56	41.2
Gender				
Male	212	73.6	80	58.8
Female	76	26.4	56	41.2
Pathological Stage				
I	179	62.2	–	–
II	25	8.7	–	–
III	51	17.7	–	–
IV	15	5.2	–	–
Unknown	18	6.2	–	–
T stage				
T1	199	69.1	80	58.8
T2	36	12.5	18	13.2
T3	47	16.3	35	25.8
T4	2	0.7	3	2.2
Unknown	4	1.4		
N stage				
N0	143	49.7	116	85.3
N1	24	8.3	3	2.2
N2	3	1	–	–
Unknown	118	41	17	12.5
M stage				
M0	205	71.2	120	88.2
M1	9	3.1	14	10.3
Unknown	74	25.7	2	1.5

suppression roles in RCC progress [18]. Notably, combining ICIs and traditional targeted drugs has presented superior tumor suppression efficacy. For example, a recently published meta-analysis has indicated better survival outcomes of metastatic RCC patients who underwent the combined therapy of ICIs and tyrosine kinase inhibitors (TKIs) [19]. Another clinical trial on the combined therapy of Pembrolizumab and Axitinib presented better anti-tumor activity and acceptable adverse effects in advanced RCC patients [20]. Other common anti-tumor agents, such as Cabozantinib, also revealed their positive effects on RCC progress inhibition in first-line therapies combined with ICIs and second-line therapies [21,22]. An interesting debate has been going on about the effect of proton-pump inhibitors (PPIs) on RCC patients. Some studies pointed out that the use of PPIs may alter the response to PD-1 inhibitors and increase the risk of death [23], while some shreds of evidence showed no apparent influence of PPIs on the effects of ICIs [24]. However, as a subtype of RCC, the therapeutic strategies towards KIRP, especially advanced KIRP, are still under exploration due to the relatively small prevalence and a limited number of patients. Considering the restricted choices of therapies, there is an urgent demand for studies to explore specific drugs that can prolong the prognosis of KIRP patients. In addition to developing novel drugs, large-scale analysis of published clinical and biological data, such as omics data mining and meta-analysis, is also an effective and efficient approach for drug screening. However, many primary and clinical experiments are required to prove reliability.

In this study, we aim to explore the predictive potentials of m5C-related genes in the prognosis of KIRP patients. we performed a comprehensive analysis of the performance of m5c-related genes in KIRP patients. The detailed study pipeline is shown in Fig. 1. Three m5c factors were selected for modeling to predict the survival outcomes of patients. Moreover, further functional analyses were performed to examine the potential functions of these genes. In addition, the mutation landscapes, immune characteristics, and potential drug screenings between high and low-risk groups divided by the calculated prognostic scores were also compared and discussed.

Materials and methods

Data acquisition and processing

The transcriptome counts and corresponding clinical data were downloaded from the TCGA-KIRP cohort. 320 KIRP samples with expression profiles were obtained, including 288 tumor tissues and 32 normal tissues. Ensembl_IDs were transformed into official gene IDs based on the latest reference (GRCh38). The mean counts were selected as the expression of duplicated genes. Meanwhile, the expression data and clinical information of another 136 tumor samples were acquired from the ICGC database. The ID transformation and the elimination of duplicated genes were performed as above. The detailed clinical characteristics of these patients are summarized in Table 1.

Exploration of differentially expressed m5c-related genes

The R package "EdgeR" were applied to explore the differentially expressed genes (DEGs) between tumor and normal samples [25]. The cut-offs for DE-gene screening are $|\text{Fold Change}| \geq 2$ and p-value < 0.05. Specifically, the expression differences of 13 m5C regulators, including NSUN2, NSUN3, NSUN4, NSUN5, NSUN6, NSUN7, ALYREF, DNMT1, DNMT3A, DNMT3B, TET2, TRDMT1 and YBX1, were further examined [26]. The overall expression pattern was exhibited by volcano plot and heatmap, whereas the boxplot was used to show the differential expression of m5C regulators between tumor and normal samples.

Correlation and interaction analysis of m5c-related genes

The Search Tool for Interaction Genes (STRING) was applied to detect the protein-protein interactions between differentially expressed m5C (DE-m5C) regulators [27]. A threshold of genes at the center of the PPI network was set as a minimum gene interaction score of < 0.7. Meanwhile, we used Spearman's correlation analysis to compute the correlations between those DE-m5C regulators, the results of which were visualized by the R package "ggcorrplot."

Construction of prognosis risk model of m5C-related genes

The normalized counts of 8 DE-m5C and corresponding clinical information from KIRP samples were collected from the downloaded TGCA dataset. The R package 'glmnet' was applied to perform LASSO-penalized Cox regression for feature selection [28]. The model's penalty parameter (λ) was determined via 10-fold cross-validation based on minimum criteria. The final risk score for each sample was calculated based on the normalized expression level and the corresponding coefficient of selected factors, the formula for which was established as follows:

Table 2
All PCR primers.

Primer name	Primer sequence (5′ – 3′)
YBX1–1-F	GGGGACAAGAAGGTCATCGC
YBX1–1-R	CGAAGGTACTTCCTGGGGTTA
YBX1–2-F	CCCCAGGAAGTACCTTCGC
YBX1–2-R	AGCGTCTATAATGGTTACGGTCT
DNMT3B-1-F	CCCAGCTCTTACCTTACCATCG
DNMT3B-1-R	GGTCCCCTATTCCAAACTCCT
DNMT3B-2-F	ACCTCGTGTGGGGAAAGATCA
DNMT3B-2-R	CCATCGCCAAACCACTGGA
ALYREF-1-F	GCAGGCCAAAACAACTTCCC
ALYREF-1-R	AGTTCCTGAATATCGGCGTCT
ALYREF-2-F	TATGATCGCTCTGGTCGCAG
ALYREF-2-R	AGAGGGACGCCGTTGTACT
GAPDH-F	GTCTCCTCTGACTTCAACAGCG
GAPDH-R	ACCACCCTGTTGCTGTAGCCAA

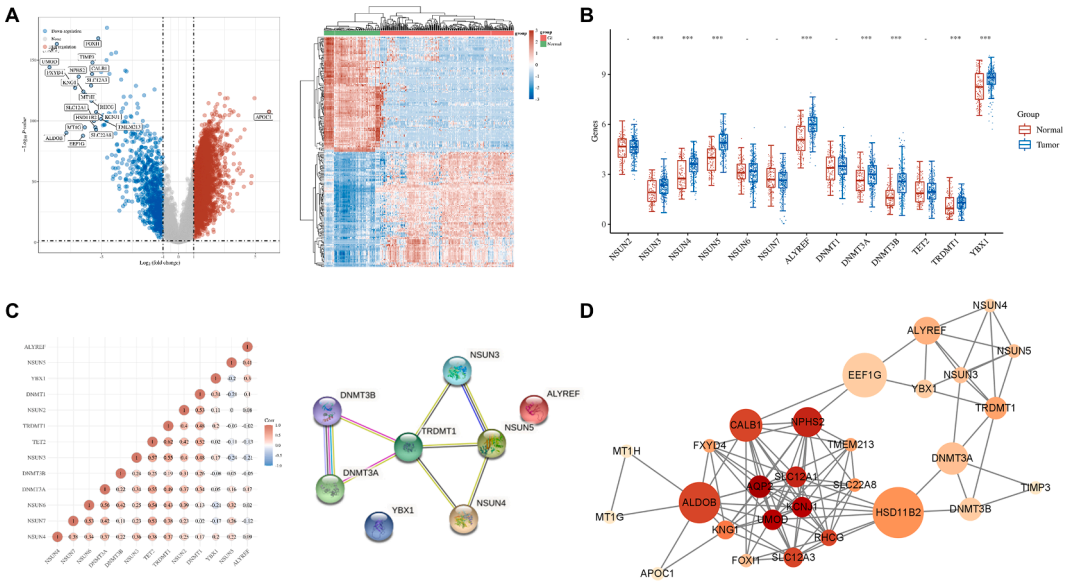

Fig. 2. the expression profiling of TCGA-KIRP cohort. (A). The volcano plot and heatmap of the overall expression. (B). The comparison of the expression level of 13 m5C related genes. (C). The correlations and interactions between m5C-related genes. (D). The interactions between DE genes and DE-m5C genes. The color of each node indicates its degree, and the size of each node represents its betweenness centrality.

$$\text{RiskScore} = \sum_{i=1}^{n} C_i * Exp_i$$

Where C_i represents the coefficient and Exp_i represents the normalized expression value of each selected m5C regulator by log2 and z-score transformation. Based on the median score in the training cohort, the KIRP patients were divided into high-risk and low-risk groups. R package 'pheatmap' was utilized to display the expression patterns of model factors from lowest risk score to highest score. The Kaplan-Meier (KM) survival analysis with the log-rank test was also performed by "survival" and "survivalminer" packages to compare the survival difference between the above two groups [29]. timeROC (v 0.4) analysis was performed to compare the predictive accuracy of this risk model on a scale of 1, 3, and 5 years [30]. Meanwhile, univariate and multivariate Cox regression was performed based on available variables to evaluate the independent prognostic value of the risk model established.

Validation of 3-gene prognostic signature in ICGC cohort

Normalized RNA-seq data and matched clinical information from the ICGC database were used for risk model validation. The cohort grouping strategy, examination of the expression patterns, exploration of survival differences, and investigation of model performance followed the same approaches described in the model construction part. In addition, the independent prognostic value of the risk model was also examined following the analysis strategy on the TCGA cohort.

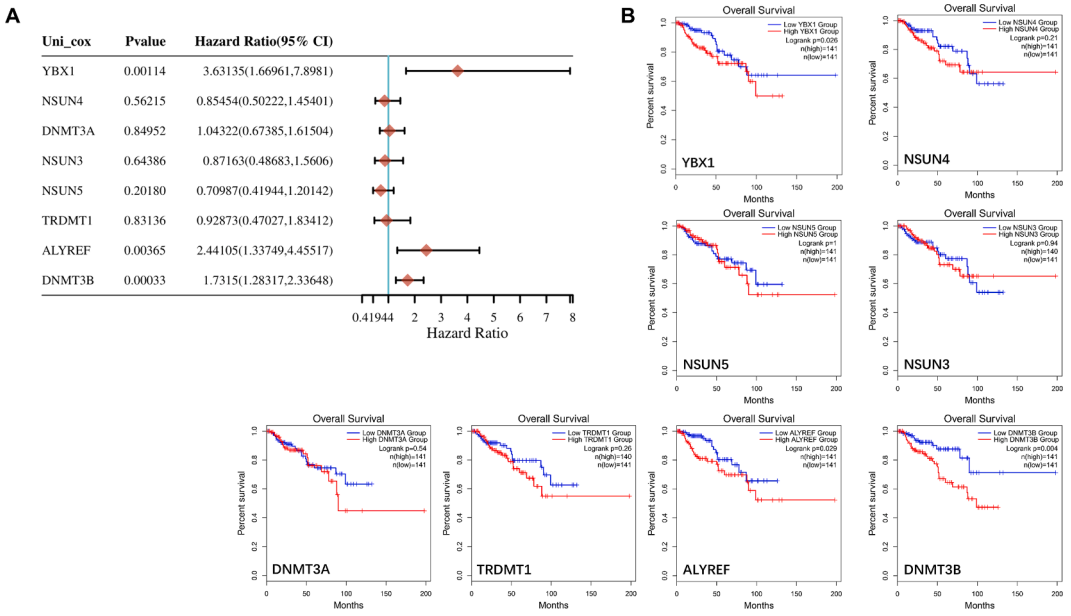

Fig. 3. The individual prognostic value of each DE-m5C regulator. (A). Forest plot showing the Hazard Ratio (95% CI) and P values for these DE-m5C regulators via univariate Cox proportional hazards analysis. (B). The Kaplan–Meier survival curves for each m5C regulator.

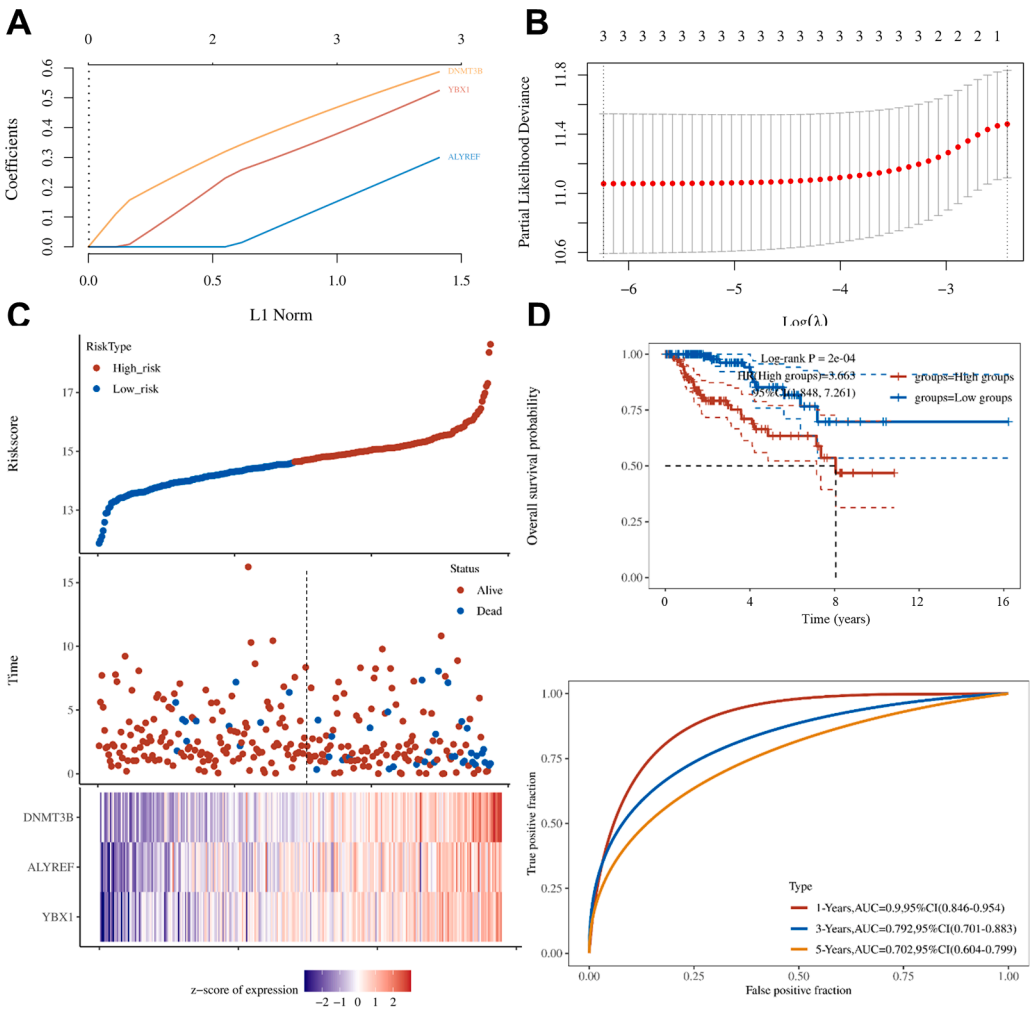

Fig. 4. The prognostic analysis towards the 3-m5c-regulator risk model in the TCGA cohort. (A). LASSO regression of the three m5C-related genes. (B). Cross-validation for optimizing the parameter in LASSO regression. (C). The distribution of risk scores and survival status of patients in these two groups. The expression trends of 3 m5C regulators were also exhibited from the lowest risk score to the highest. (D). The KM curves reflect the OS of patients in the high- and low-risk groups. (E). The time-dependent ROC curves and corresponding AUC values for the risk model in the TCGA cohort.

Functional enrichment analysis

The R package 'clusterProfiler' was applied to performing Gene Ontology (GO) AND Kyoto Encyclopedia of Genes and Genomes (KEGG) analyses on the differentially expressed genes (DEGs, $|\text{Fold Change}| \geq 2$, p-value < 0.05) between high-risk and low-risk groups [31]. The Benjamini – Hochberg method was selected to adjust the p-value. The top 10 significantly enriched ontology items and signaling pathways were visualized and retained for further literature confirmation by literature search. Besides, the overlapped ontology terms and signaling pathways were also addressed by Cytoscape software [32].

Table 3
The baseline characteristics of the patients in different risk groups.

Characteristics	TCGA cohort		
	High risk	Low risk	*P value*
Gender (%)			0.082
Female	46 (31.9)	32 (22.2)	
Male	98 (68.1)	112 (77.8)	
Age (%)			0.853
<60y	60 (41.6)	65 (45.2)	
≥60y	82 (56.9)	79 (54.8)	
Unkown	2 (1.4%)	0 (0)	
Race			0.785
American Indian or Alaska Native	0 (0)	2 (1.4)	
Asian	5 (3.5)	2 (1.4)	
Black or African American	32 (22.2)	30 (20.8)	
White	100 (69.4)	102 (70.8)	
Unkown	7 (4.9)	8 (5.6)	
TNM Stage (%)			0.006
I+II	110 (76.4)	122 (84.7)	
III+IV	34 (23.6)	22 (15.3)	

Examination of mutation and immune characteristics

The R package named "maftools" was applied to compare mutation differences between high and low-risk groups [33]. The top 5 mutant genes were selected for detailed literature exploration in PubMed. The "CIBERSORT" package is a robust tool for evaluating immune infiltration, which was utilized here to estimate the proportions of immune-related cells in two groups. Besides, The Stromal score and immune score were also calculated via the "ESTIMATE" package. We also used the "TIDE" method to compare the effectiveness of immunotherapies on patients in these two groups, and the expression levels of two immune checkpoints, including PD-1 and CTLA-4, were also examined.

Drug sensitivity analysis and small-molecule drugs screening

"pRRophetic," an R package for drug response prediction based on an expression matrix, was used to explore the sensitivity differences of commonly used anti-cancer drugs between high and low-risk groups [34]. In addition, the connectivity map (cMAP) database, which contains gene expression profile changes caused by 33,609 small molecule compounds based on multiple cell lines, was also applied to screen potentially effective small molecules [35]. A threshold of the score was

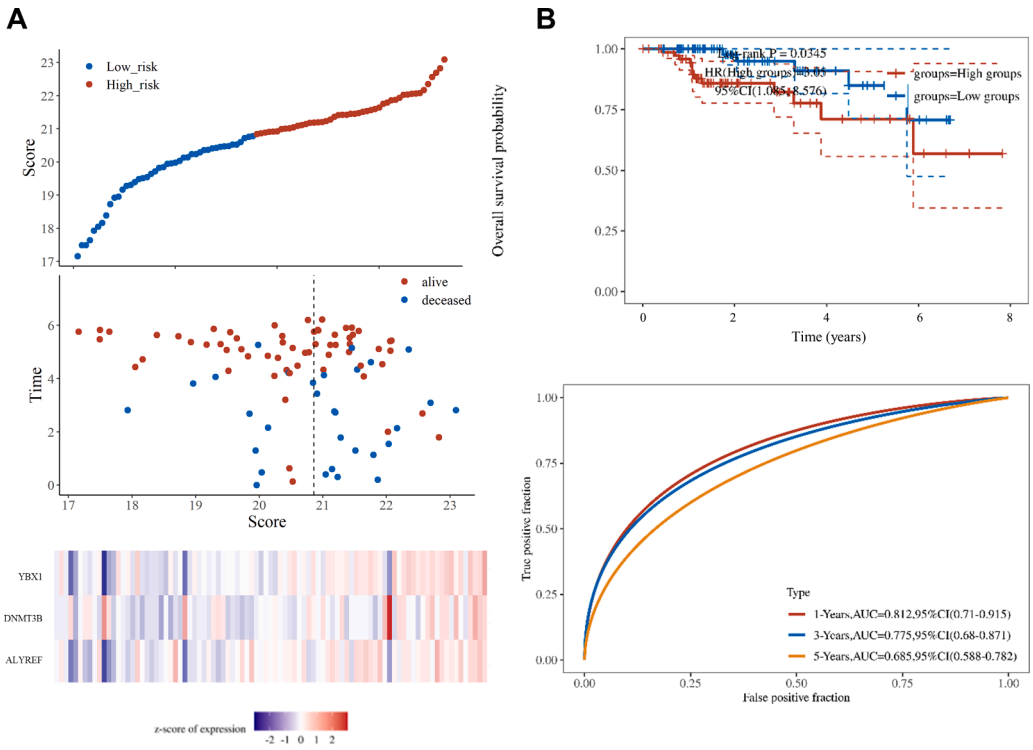

Fig. 5. The validation of the 3-gene prognostic model in the ICGC cohort. (A). The distribution of risk scores in the ICGC cohort (up). The 3-m5C regulator expression patterns (left to right): low risk to high risk (down). (B). The KM survival curves for the OS of patients in the high- and low-risk groups (up). The time-dependent ROC curves and related AUC of the risk model in the ICGC cohort (down).

set as −0.6 to select the most promising compounds. Those satisfying candidates' chemical information and structures were further explored in PubChem and PubMed databases.

Cell culture

The HK-2 and Caki-2 cell lines were obtained from Pricella (Wuhan, China), which were further cultured at 37 °C and 5% CO2 in 1640 medium (Gibco) supplemented with 10% fetal bovine serum (FBS, Gibco) and 1% penicillin-streptomycin (Gibco). Once the cells reached 80% confluence, they were subcultured using 0.25% trypsin and 0.02% ethylene-diamine-tetra-acetic acid (EDTA, Gibco) for further passages.

Quantitative real-time PCR

Total RNA was isolated using TRIzol reagent (Nanjing Vazyme Biotech Co., Ltd.). 1 μg of total RNA was reverse-transcribed with SuperScript III transcriptase (Nanjing Vazyme Biotech Co., Ltd.). Quantitative real-time PCR (qRT-PCR) was performed using a qTOWER (Chen et al., 2020) G system (Analytik Jena, Germany) with SYBR Green to measure the mRNA expression levels of the gene of interest. GAPDH was used as a reference gene for normalization (see Table 2 for detailed

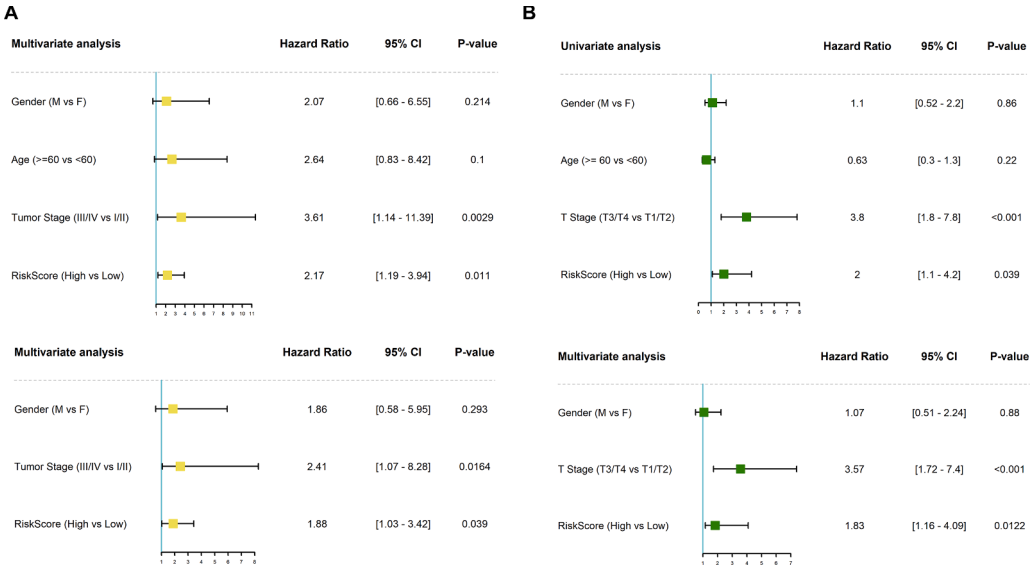

Fig. 6. Results of the univariate and multivariate Cox regression on the OS in the TCGA and ICGC cohort. (A). TCGA. (B). ICGC.

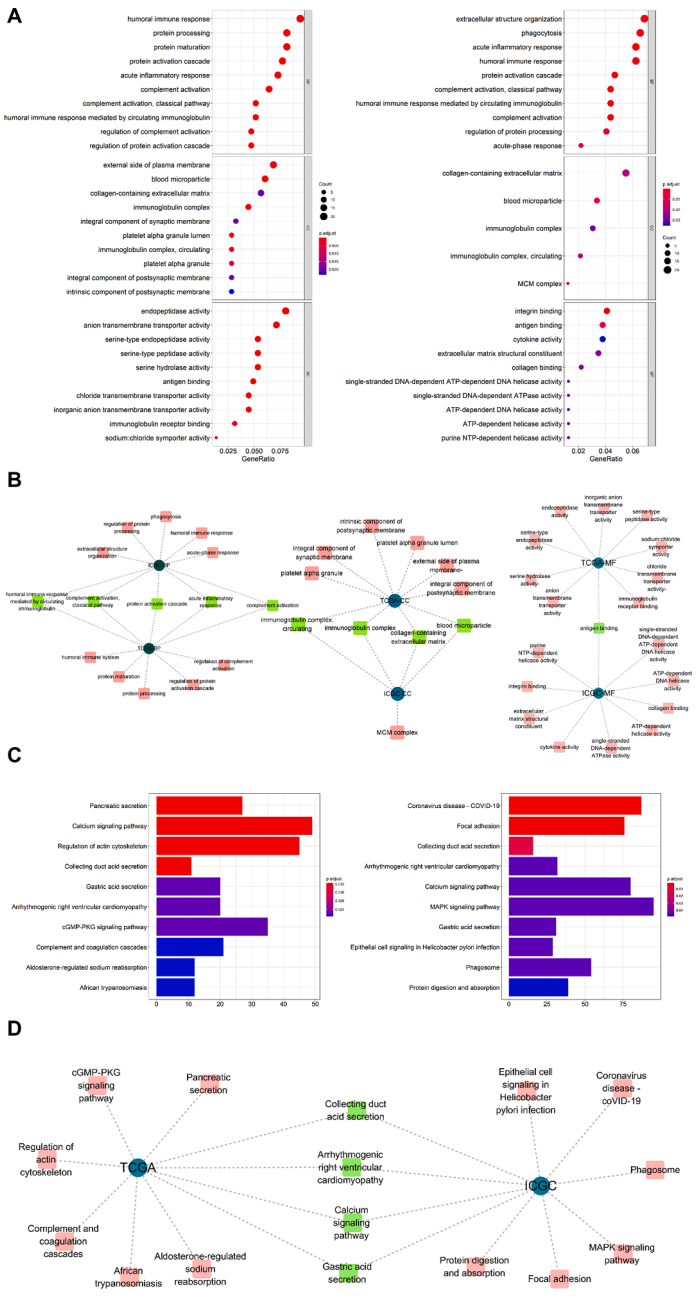

Fig. 7. Results of functional enrichment analysis. (A). The most significantly enriched GO items of the TCGA (left) and ICGC (right) cohort. (B). The GO items which were appeared in both analyses. (C). For the most significantly enriched KEGG signaling pathways, the left bar chart represents the TCGA cohort, whereas the right one is the ICGC cohort. (D). The KEGG signaling pathways were mapped in both cohorts.

sequences). Measurements were performed in triplicate, and the results were analyzed using the 2−ΔΔCt method for relative quantification. A list of primers designed for qRT-PCR is shown in Table 2.

Statistical analysis

All statistical analyses and used R packages were implemented by the R foundation for statistical computing (2020) version 4.0.3. If not specified above, a P-value less than 0.05 was considered statistically significant, and all P values were two-tailed.

Results

The exploration of DE-genes and m5C regulators in KIRP

Totally, we identified 5950 differentially expressed (DE) genes, among which 5151 are up-regulated, whereas 799 are down-regulated. The general expression landscape was visualized in Fig. 2A, where the most significant DEGs were labeled. Notably, we examined the expression of m5C-related regulators, and 8 out of 13 were differentially expressed, including NSUN3, NSUN4, NSUN5, ALYREF, DNMT3A, DNMT3B, TRDMT1, and YBX1 (Fig. 2B). A correlation analysis was conducted to determine the crosstalk among these m5C regulators, which revealed that most of the m5C regulators are positively correlated (Fig. 2C). Notably, TRDMT1 has the strongest positive correlations with most other regulators, whereas the correlations between ALYREF and

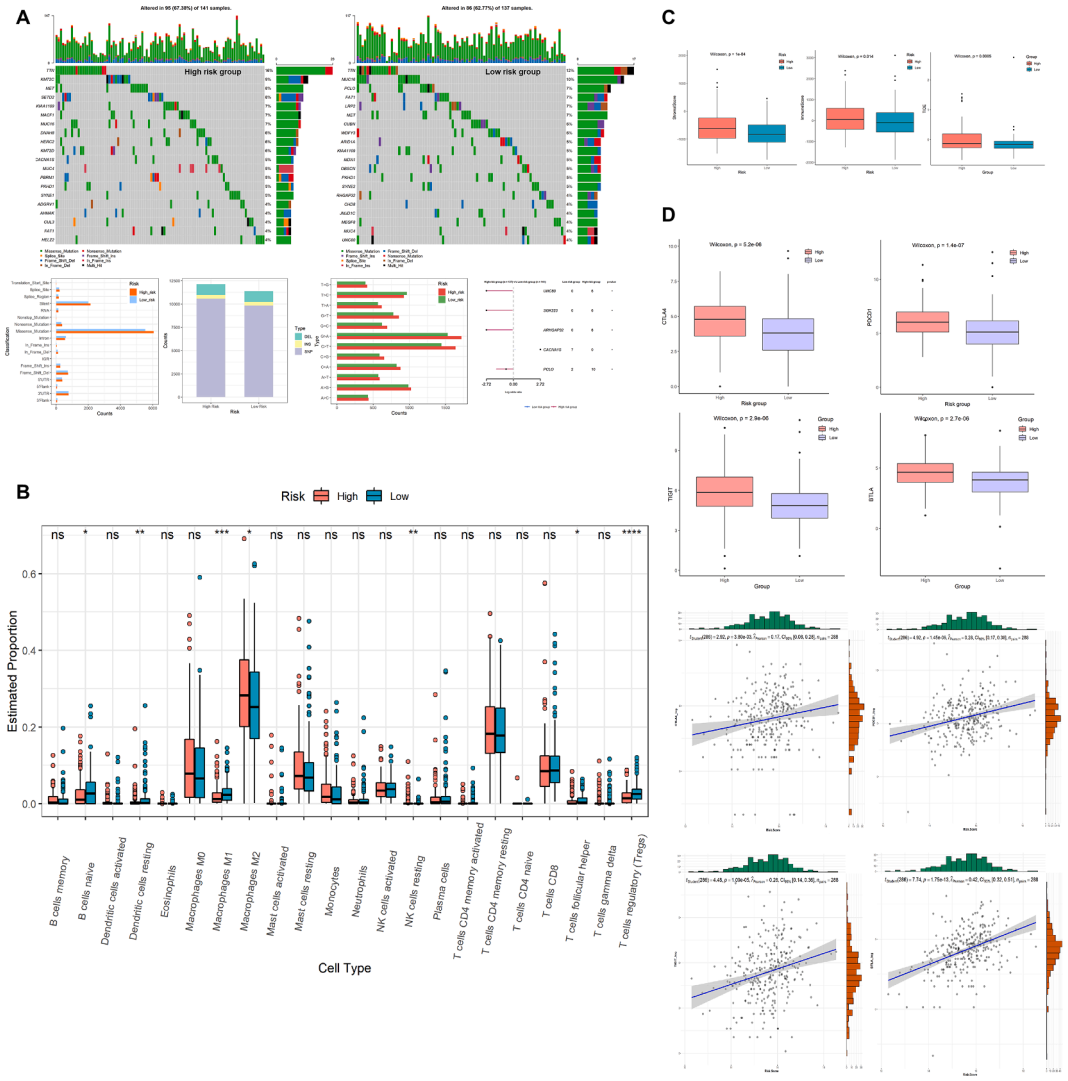

Fig. 8. The mutation and immune characterizations of high- and low-risk groups. (A). The comparison of mutation landscapes. (B). The proportions of immune cells in these two groups. (C). The evaluation of tumor immune microenvironment. (D). The comparison and correlations of immune checkpoints between high- and low-risk groups.

other regulators are pretty weak, most of which are negative. Further protein-protein interaction analysis demonstrated TRDMT1 as the hub gene, suggesting that the DNMT family interacts with the NSUN family indirectly via TRDMT1 (Fig. 2C). ALYREF, however, has no significant interactions with those regulators. Pieces of evidence have indicated the critical roles of TRDMT1 in cancer pathogenesis. For example, Bloniarz et al. noticed that lacking TRDMT1 and DNMT2 will reduce the cell apoptosis rate in glioblastoma [36]. Meanwhile, A recent study showed that the knock-out of TRDMT1 may increase cancer's cellular and genetic heterogeneity [37]. Besides, hyper ubiquitination of TRDMT1, which decreases its expression, may suppress the process of homologous recombination [38]. In addition to examining m5C inner interactions, we also constructed the interaction network between DE-m5C regulators and the most significant DEGs to determine the associations between DE-m5C regulators and DEGs of KIRP. Fig. 2D shows that these genes are divided into 2 clusters, as expected. Four genes, including AQP2, UMOD, KCNJ1, and SLC12A1, have the strongest degree among the network, indicating their indispensable roles in renal lesion and KIRP development [39–42]. EEF1G and HSD11B2, the two main mediators, connect the KIRP-related and m5C clusters. Previous evidence has revealed a negative correlation between HSD11B2 and DNMT3A, and the upregulation of DNMT3A and DNMT3B may increase the invasiveness of tumors and promote angiogenesis [43]. The expression profiling results have suggested a close relationship between m5C-related genes and KIRP pathogenesis, indicating their promising roles in KIRP diagnosis and prognosis evaluation.

Individual prognostic values of DE-m5C-related regulators

Through univariate Cox regression, we measured the prognostic value of the 8 DE-m5C related genes, respectively, which were visualized in Fig. 3A. Three items, including YBX1, ALYREF, and DNMT3B, are significantly correlated with patient outcomes, and all of these three genes were identified as poor prognostic factors (Hazard Ratio > 1). Furthermore, KM survival analysis also showed significantly different overall survival (OS) between high and low expression of such three genes, respectively (Fig. 3B). However, the individual prognostic value of the rest m5C regulators is slightly feeble. These results suggest the predictive potentials of these three m5C regulators in the KIRP prognosis.

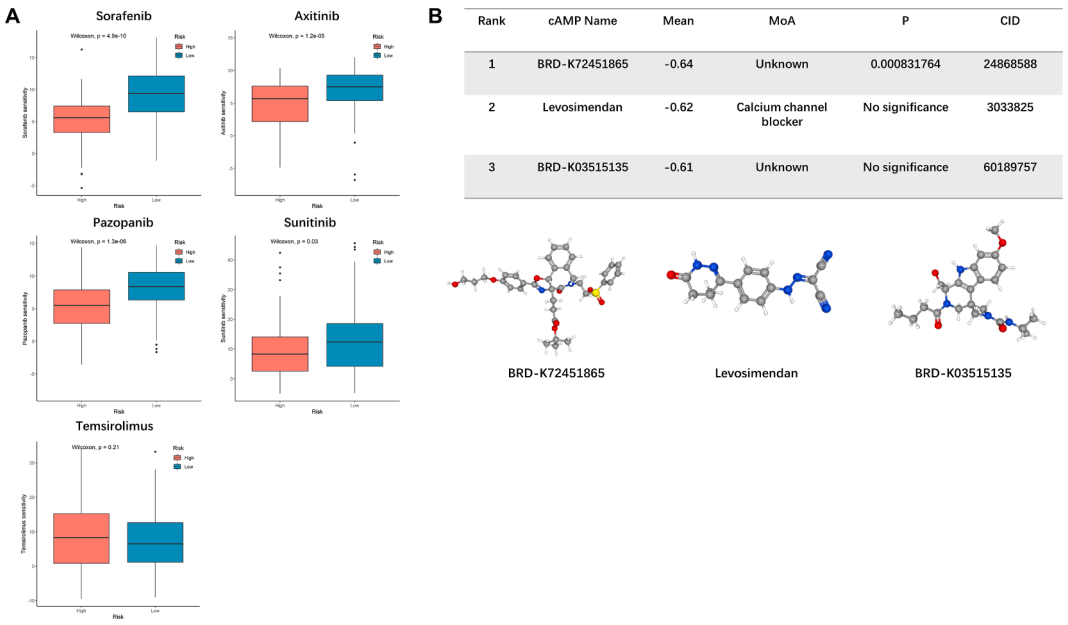

Rank	cAMP Name	Mean	MoA	P	CID
1	BRD-K72451865	-0.64	Unknown	0.000831764	24868588
2	Levosimendan	-0.62	Calcium channel blocker	No significance	3033825
3	BRD-K03515135	-0.61	Unknown	No significance	60189757

Fig. 9. The results of drug sensitivity testing and screening of potentially effective small compounds. (A). The comparison of drug sensitivities between high- and low-risk groups. (B). The potential effective small molecules for high-risk groups.

Construction and validation of m5C-based signature in KIRP patients

We first evaluated the predictive performance of single m5C regulators in KIRP prognosis via ROC analyses. The area under the curve (AUC) of the three m5C regulators obtained in the last step was calculated and shown in Supplementary Fig. 1. Our analyses indicate that a single m5C regulator is not sufficient and stable for the prognosis prediction of KIRP (AUC ranges from 0.489 to 0.729). Considering their contributions to the evolution of KIRP and the subpar performance of a single predictor, an integrated risk model for prognosis assessment is demanded construction.

We applied LASSO Cox regression to the three m5C-related genes to establish a prognostic model based on their expression profile. As a result, a 3-regulator signature was identified according to the optimal value of λ (Fig. 4A, B). the detailed calculative formula of risk score is shown below:

$$Risk\ score = (0.2993)^{*}\ ALYREF_{exp} + (0.5872)^{*}\ DNMT3B_{exp} + (0.5243)^{*}YBX1_{exp}$$

Here, the *exp* means the expression level of a specific gene. Based on the median cut-off value (Fig. 4C), the patients were stratified into a high-risk group ($n = 144$) and a low-risk group ($n = 144$). Before further analyses, we examined the expression of such three m5C regulators via immunocytochemistry analysis in The Human Protein Atlas (HPA), the results of which showed higher expression of these genes in kidney tissue (Supplementary Fig. 1). Subsequently, the baseline characteristics were compared between the high and low-risk groups, and the results are shown in Table 3. Although no significant differences in age, race, and gender were noticed between these two groups, patients in the high-risk group tend to have more advanced TNM stages.

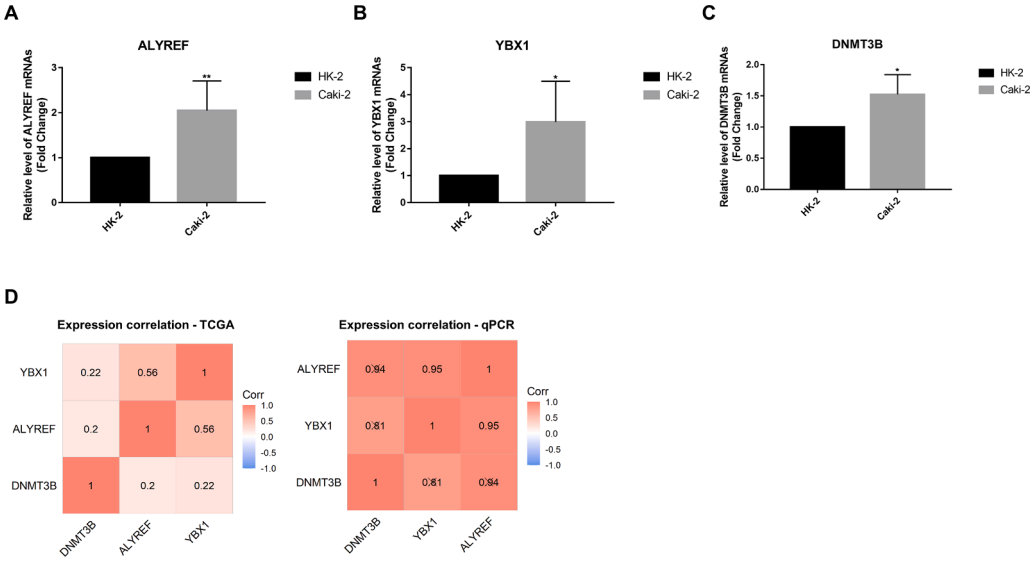

Fig. 10. Expression validation of 3 m5C genes of the risk score model. (A-C). The relative expression data of ALYREF, YBX1, and DNMT3B. (D). The expression correlation heatmap is based on TCGA (left) and qPCR (right) data.

Meanwhile, more dead cases were identified in the high-risk group, indicating a higher possibility of an earlier death of patients in the high-risk group (Fig. 4E). KM survival curve also showed similar outcomes, where the OS of patients in the high-risk group is significantly worse than those in the low-risk group (Fig. 4D). Finally, the time-dependent ROC curves and the values of AUC were drawn and calculated to evaluate the predictive performance of our model. Results showed that the AUC reaches 0.9 at one year, 0.792 at three years, and 0.702 at five years, respectively (Fig. 4F).

To further validate the generalization capability of our model, we also applied this model to the prognostic analysis of the ICGC cohort. The median of the risk score was used to divide the patients into high- and low-risk groups. Results of this analysis have shown similar prognostic patterns to that of the TCGA cohort. In detail, patients in the high-risk group have a higher probability of earlier death. Most of the m5C regulators involved in this model showed lower expressions in patients of the low-risk group (Fig. 5A). The KM survival test also showed poorer prognostic outcomes of patients in the high-risk group (Fig. 5B). In addition, the AUC of our model for this cohort is 0.812 at one year, 0.775 at three years, and 0.685 at five years (Fig. 5B), which are generally acceptable. In summary, the outcomes of the presented analysis further confirmed an excellent predictive capability for the prognosis of KIRP patients.

Evaluation of independent prognostic value of risk model

We applied univariate and multivariate Cox regression to the available variables of both the TCGA and ICGC cohorts to assess the independent predictor potential of the risk score. The results of the univariate regression revealed a significant association between our risk model and OS in these two cohorts (TCGA: HR=2.17, 95% CI=1.19 – 3.94, *p-value*=0.011; ICGC: HR=2, 95% CI=1.1 – 4.2, *p-value*=0.039). Furthermore, with the correction from other confounding factors, the outcomes of multivariate Cox regression also indicated the risk score as an excellent independent predictor for OS (TCGA: HR=1.88, 95% CI=1.03 – 3.42, *p-value*=0.039; ICGC: HR=1.83, 95% CI=1.16 – 4.09, *p-value*=0.0122). The detailed results of both univariate and multivariate Cox regression are visualized in Fig. 6.

Functional enrichment analyses in TCGA and ICGC cohort

Functional enrichment analyses, including signaling pathway and gene ontology (GO), were performed in both TCGA and ICGC cohorts to examine the biological functions of DE genes between high- and low-risk groups. As shown in Fig. 7, eight GO items and four signaling pathways were mapped in both cohorts. Also, those DE genes are significantly enriched in some epigenetic modification signaling pathways and ontology terms, as expected, such as calcium signaling, MAPK signaling, regulation of protein processing, and so on [44,45]. In addition, the DE genes from both cohorts were also apparently enriched in immune-related pathways and GO items, including humoral immune response, acute immune response, immunoglobulin complex, and cytokine activity, which indicates the different immune landscapes between these two groups. These results may partially explain the different OS outcomes between these two groups, and standard therapies' treatment efficacies might also differ.

Mutation analysis and immune characterization

To further excavate the biological differences between high- and low-risk groups, we also checked the mutation landscapes in the TCGA cohort, the detailed results of which were visualized in Fig. 8A. It is observed that the mutation occurrence is more frequently seen in the high-risk group, where mutation counts and types are significantly higher than that in the low-risk group. Five genes with the most significant differences in their mutation frequencies were calculated between these two groups, including UNC80, SGK223, ARHGAP32, CACNA1S, and PCLO. Only CACNA1S have significantly higher mutation frequency in the low-risk group. Literature mining from PubMed indicated that UNC80 regulates the transportation of small molecules, the mutation of which may influence the prognosis of cancer patients [46].

Moreover, evidence also pointed out that SGK223 is closely associated with tumor cell proliferation [47]. Furthermore, ARHGAP32 is considered a potential metastasis suppression gene in melanoma [48], and it was already selected as a critical factor for predicting the prognosis of gastric cancer [49]. In addition, the mutation of PCLO may promote the pathogenesis of multiple cancers, such as colon cancer and hepatocellular carcinoma [50,51].

Based on the functional enrichment analysis outcomes, both groups' immune characterizations were investigated. The examination of the immune cell proportions showed a significantly higher amount of M2 macrophages in the high-risk group. However, the proportions of B cell naïve, dendritic cells resting, macrophage M1, NK cell resting, T cell follicular helper, and Tregs are obviously lower than the low-risk group (Fig. 8B). Furthermore, the tumor immune microenvironment analysis revealed a significantly higher association between patients in the high-risk group and stromal score and immune score (p-value=1e-04 and p-value=0.014, respectively, Fig. 8C)). Meanwhile, the patients in the high-risk group also have a higher possibility of tumor immune escape based on the results of TIDE, which was further supported by the higher expression of immune checkpoints, including PDCD-1, CTLA-4, TIGIT, and BTLA (Fig. 8D). Besides, the Pearson correlation analysis also exhibited a positive-correlations between risk scores and the expression levels of these checkpoints.

Comparison of drug sensitivities and prediction of effective small compounds

Finally, five commonly used anti-cancer drugs, including Sorafenib, Axitinib, Pazopanib, Sunitinib, and Temsirolimus, were tested for sensitivities in these two groups (Fig. 9A). The data showed that patients in the low-risk group responded to most of these drugs more positively (Sorafenib: *p-value*=4.9e-10; Axitinib: *p-value*=1.2e-05; Pazopanib: *p-value*=1.3e-06; Sunitinib: *p-value*=0.03). It seems that Temsirolimus works better towards patients in the high-risk group, although the sensitivity is not statistically significant (*p-value*=0.21). We also applied the cMAP platform to screen the potentially effective small molecules for patients in the high-risk group. Totally, three small molecules were obtained (Fig. 9B). The detailed mechanisms of 2 of these small molecules are still under investigation. It is noticed that Levosimendan, an effective compound for heart failure treatment and rarely discussed in cancer treatment, was also considered by cMAP calculation, possibly due to its role in blocking the calcium channel.

Experimental validation by qPCR

We validate expression analysis through qPCR tests on three m5C genes in Caki-2 and HK-2 cell lines (Fig. 10A, B, and C). The results revealed that the expression of ALYREF was significantly increased in Caki-2 cell lines ($p<0.01$). In addition, DNMT3B and YBX1 were up-regulated significantly ($p<0.05$). These are consistent with our bioinformatics analysis results. Furthermore, we conducted correlation analysis on these genes using both TCGA and qPCR data, which showed a significantly positive correlation in their expression. However, only ALYREF and YBX1 demonstrated a statistically significant positive correlation in the qPCR data (Fig. 10D).

Discussion

As one of the main epigenetic modification types, m5C has drawn increasing attention in recent years. Although scattered studies have

demonstrated that some vital m5C genes have been presented [52–54], a systematic analysis for illustrating m5C events in KIRP is highly demanded. In this study, we examined the expression of m5C-related regulators in KIRP samples and systematically investigated the relationship between these regulators and the OS of KIRP patients. Via applying LASSO regression, we successfully established a 3-m5C gene-based prediction model for KIRP prognosis, further validated by an external dataset. The survival analyses showed significant differences in OS between high- and low-risk groups that were divided based on the risk scores.

Moreover, the roles of each m5C regulator involved in our model were further investigated via literature mining. For example, it is pointed out that YBX1 will promote cancer cell adhesion, migration, and invasion [55], which finally leads to the acceleration of cancer metastasis. Meanwhile, DNMT3B and DNMT3A are essential regulators in kidney development. The genomic regions regulated by these two genes are potent enhancers for cell proliferation, suggesting that their dysregulation may lead to aberrant cell cycles in the kidney [56]. In addition, the upregulation of ALYREF also enhances tumor cell proliferation and modifies the immune microenvironment [57]. Taken together, the genes involved in our model are closely related to cancer and kidney-related development, further supporting its feasibility and reliability.

Through the univariate and multivariate Cox regression, we have demonstrated superior predictive efficacy of our model for both short-term and long-term prognosis compared to single-factor-based prognosis evaluation. To explore the potential biological functions, functional enrichment analyses of the DE genes between high- and low-risk groups were also performed, which indicated the differences in m5C regulation and immune responses. Subsequently, the genomic mutations and immune characterizations were also explored to determine the potential reasons for the differences obtained in enrichment analyses. We noticed that patients in the high-risk group might face higher frequent mutations, and the methylation modification rates are also elevated. The immune cell proportion estimation showed increased M2 macrophages, indicating the severer tumor status, such as promoted cell proliferation and enhanced angiogenesis, in the high-risk group [58]. Following immune scoring revealed a poor tumor microenvironment in the high-risk group, including higher stromal cell rates and increased risk of immune escape. These results suggested a promising performance of our risk model and emphasized the role of m5C in regulating KIRP development. Finally, we also examined several common-used drugs. The outcomes of our analysis showed better performance of most of our selected drugs in the low-risk group. Through the cMAP prediction, we identified several potentially effective small molecules for patients in the high-risk group. However, large-scale mechanism investigations and clinical trials are still required for validation.

To date, an increasing number of prognostic models based on expression profiles have been put forward in cancer research, including ferroptosis-based [59], pyroptosis-based [60], m6A-based [61], and necroptosis-based risk models [62], all of which have shown excellent performance in the evaluation and prediction of cancer prognosis. However, there are still some limitations. The key problem is that no further validations are performed to examine these models' robustness and general applicability, the clinical application of which, in other words, is still ambiguous. Moreover, clinicians may encounter a dilemma when choosing such models in clinical usage: Which models are more suitable for the prognostic evaluation? Or, under what conditions does a specific model have perfect performance? Ren et al. have built an integrative knowledge base where more than 800 risk models are included and compared, which have set a good reference for model selection [63].

Interestingly, their study also found that the accuracy of some of the published models decreased obviously when applied to another dataset. Therefore, it is urgent to conduct relevant investigations, or clinical trials, focusing on such problems, to systematically assess these risk models based on a larger scale of real-world data. Meanwhile, efforts could be made to integrate the models of the same cancer types, perhaps enhancing the accuracy and applicability of prognostic prediction and assessment. Lastly, cancer has a highly complex system, which brings about considerable difficulties in diagnosis, treatment, and prognosis. Thus, clinicians typically measure the disease status of patients from multi-level data, such as imaging, physiological, and genomic data. An integrative analysis of such data may provide a more comprehensive understanding of the patients, and the efficiency and accuracy of diagnoses could also be improved. Nowadays, more and more researchers have put their efforts into developing novel algorithms and strategies for multi-level data integration. Especially during the COVID-19 pandemic, lots of newly developed methods have been put forward to assist the track and diagnosis of SARS-Cov-2 infection, data involved in which include CT imaging, results of nucleic acid and antibody testing, genomic sequences, as well as social connection data [64–67].

The significance of the presented study can be summarized below. First, our study further confirmed the roles of m5C regulators in KIRP. Combined with their proven roles in regulating proliferation and homologous recombination of cancer cells, the explorations of genomic mutation, protein-protein interaction, immune characterizations of different risk groups, and drug responses in this study may provide new insights for future m5C-related mechanism investigation of KIRP. Second, our model has demonstrated its good performance in evaluating KIRP prognosis, based on which a more complex but more accurate and robust model could be established with the involvement of clinical records and image data in the following studies. Lastly, the investigation and modeling pipeline could give a paradigm for researchers who will explore m5C regulators and construct related diagnosis or prognosis models for other complex diseases.

Several limitations remain in this study. Firstly, our prognostic model was constructed and validated based on the data from publicly available databases. However, more real-world data are demanded further to confirm its practical clinical utility in the future. Meanwhile, we only examined the differences in the immune system and genetic mutations between the high- and low-risk groups. Therefore, these two groups' molecular mechanisms, detailed clinical features, and precise treatments are still unclear. In particular, it is still unknown why patients in the high-risk group showed poorer responses to immunotherapy. This should be addressed explicitly in future studies to provide more reliable evidence, and novel therapeutic strategies could be developed according to these findings. In addition, the drugs screened as potential therapies for KIRP should be further validated. Finally, the robustness and applicability of this model are still limited, as many essential genes closely related to the KIRP prognosis were excluded.

In conclusion, this study has established a novel prognostic model based on three m5C-related genes. Furthermore, this model demonstrated its independent association with the overall survival of KIRP patients in derivation and validation cohorts, which may provide new insights for predicting and evaluating KIRP prognosis. However, the mechanisms of m5C-related genes in KIRP pathogenesis and related immune activity remain poorly understood and need further addressing.

Ethics approval and consent to participate

Not applicable.

Consent for publication

Not applicable.

Availability of data and materials

Publicly available datasets were analyzed in this study. This data can be found here: (1) https://portal.gdc.cancer.gov/. (2) https://dcc.icgc.org/.

Declaration of Competing Interest

The authors declare the following financial interests/personal relationships which may be considered as potential competing interests:

RKS is having honorary based association with iGlobal Research and Publishing Foundation, New Delhi India, who declare that there are no conflicts of interest. The remaining authors declare that the research was conducted in the absence of any commercial or financial relationships that could be construed as a potential conflict of interest.

Funding

This work was supported by the Health Commission of Henan Province (Grant number: LHGJ20190665) and the 2020 Medical Science and Technology Research Plan of Henan Province (key project jointly built by Henan Province and National Ministry, grant number: SBGJ202002023).

Acknowledgments

We thank all the members of Dr. Zhen Zhang's lab and various colleagues in the Department of Anesthesiology for their assistance and/or scientific discussion.

Supplementary materials

Supplementary material associated with this article can be found, in the online version, at doi:10.1016/j.tranon.2023.101741.

References

[1] H. Sung, et al., Global cancer statistics 2020: globocan estimates of incidence and mortality worldwide for 36 cancers in 185 countries, CA Cancer J. Clin. 71 (3) (2021) 209–249.
[2] J. Deng, et al., A comparison of the prognosis of papillary and clear cell renal cell carcinoma: evidence from a meta-analysis, Medicine 98 (27) (2019) e16309. Baltimore.
[3] A. Brozovich, et al., All bone metastases are not created equal: revisiting treatment resistance in renal cell carcinoma, J. Bone Oncol. 31 (2021), 100399.
[4] M. Roberto, et al., Metastatic renal cell carcinoma management: from molecular mechanism to clinical practice, Front. Oncol. 11 (2021), 657639.
[5] Q. Li, et al., Nsun2-mediated M5c methylation And mettl3/mettl14-mediated m6a methylation cooperatively enhance p21 translation, J. Cell. Biochem. 118 (9) (2017) 2587–2598.
[6] B.S. Zhao, I.A. Roundtree, C. He, Post-transcriptional gene regulation by mrna modifications, Nat. Rev. Mol. Cell Biol. 18 (1) (2017) 31–42.
[7] S. Dong, et al., N(6) -methyladenosine steers rna metabolism and regulation in cancer, Cancer Commun. 41 (7) (2021) 538–559. Lond).
[8] H. Shen, et al., The emerging roles of n6-methyladenosine rna methylation in human cancers, Biomark. Res. 8 (2020) 24.
[9] B. Zhang, et al., M(6)A target micrornas in serum for cancer detection, Mol. Cancer 20 (1) (2021) 170.
[10] B. Linder, et al., Single-nucleotide-resolution mapping of m6a and m6am throughout the transcriptome, Nat. Methods 12 (8) (2015) 767–772.
[11] A.B.R. McIntyre, et al., Limits in the detection of M(6)A changes using merip/M(6) A-Seq, Sci. Rep. 10 (1) (2020) 6590.
[12] X. Chen, et al., 5-Methylcytosine promotes pathogenesis of bladder cancer through stabilizing Mrnas, Nat. Cell Biol. 21 (8) (2019) 978–990.
[13] H. Yang, et al., FMRP Promotes transcription-coupled homologous recombination via facilitating Tet1-mediated M5c Rna modification demethylation, Proc. Natl. Acad. Sci. U. S. A. 119 (12) (2022), e2116251119.
[14] T. Liu, et al., 5-Methylcytosine Rna methylation regulators affect prognosis and tumor microenvironment in lung adenocarcinoma, Ann. Transl. Med. 10 (5) (2022) 259.
[15] W. Xu, et al., Integrative 5-methylcytosine modification immunologically reprograms tumor microenvironment characterizations and phenotypes of clear cell renal cell carcinoma, Front. Cell Dev. Biol. 9 (2021), 772436.
[16] Y. Liu, et al., Identification of the expression patterns and potential prognostic role of 5-methylcytosine regulators in hepatocellular carcinoma, Front. Cell Dev. Biol. 10 (2022), 842220.
[17] Z. Huang, et al., Construction of prognostic risk model of 5-methylcytosine-related long non-coding rnas and evaluation of the characteristics of tumor-infiltrating immune cells in breast cancer, Front. Genet. 12 (2021), 748279.
[18] N. Chowdhury, C.G. Drake, Kidney cancer: an overview of current therapeutic approaches, Urol. Clin. North Am. 47 (4) (2020) 419–431.
[19] A. Rizzo, et al., Impact of clinicopathological features on survival in patients treated with first-line immune checkpoint inhibitors plus tyrosine kinase inhibitors for renal cell carcinoma: a meta-analysis of randomized clinical trials, Eur. Urol. Focus 8 (2) (2022) 514–521.
[20] M.B. Atkins, et al., Axitinib in combination with pembrolizumab in patients with advanced renal cell cancer: a non-randomised, open-label, dose-finding, and dose-expansion phase 1b trial, Lancet Oncol. 19 (3) (2018) 405–415.
[21] M. Santoni, et al., Cabozantinib in patients with advanced renal cell carcinoma primary refractory to first-line immunocombinations or tyrosine kinase inhibitors, Eur Urol Focus (2022).
[22] R. Flippot, et al., Therapeutic sequencing in the era of first-line immune checkpoint inhibitor combinations, a novel challenge in patients with metastatic clear-cell renal cell carcinoma, Bull. Cancer 109 (2S) (2022) 2S31–2S38.
[23] Q. Giordan, et al., Impact of antibiotics and proton pump inhibitors on efficacy and tolerance of anti-pd-1 immune checkpoint inhibitors, Front. Immunol. 12 (2021), 716317.
[24] V. Mollica, et al., Concomitant proton pump inhibitors and outcome of patients treated with nivolumab alone or plus ipilimumab for advanced renal cell carcinoma, Target Oncol 17 (1) (2022) 61–68.
[25] Y. Chen, A.T. Lun, G.K. Smyth, From reads to genes to pathways: differential expression analysis of rna-seq experiments using rsubread and the edger quasi-likelihood pipeline, F1000Res 5 (2016) 1438.
[26] H. Zhou, et al., The role of m5c-related lncrnas in predicting overall prognosis and regulating the lower grade glioma microenvironment, Front. Oncol. 12 (2022), 814742.
[27] D. Szklarczyk, et al., String V11: protein-protein association networks with increased coverage, supporting functional discovery in genome-wide experimental datasets, Nucleic. Acids. Res. 47 (D1) (2019) D607–D613.
[28] J.H. Friedman, T. Hastie, R. Tibshirani, Regularization paths for generalized linear models via coordinate descent, J Stat Softw 33 (1) (2010) 1–22.
[29] T. Therneau, P. Grambsch, Modeling Survival Data: Extending the Cox Model, Springer, New York, 2000.
[30] P. Blanche, J.F. Dartigues, H. Jacqmin-Gadda, Estimating and comparing time-dependent areas under receiver operating characteristic curves for censored event times with competing risks, Stat. Med. 32 (30) (2013) 5381–5397.
[31] T. Wu, et al., Clusterprofiler 4.0: a universal enrichment tool for interpreting omics data, Innovation 2 (3) (2021), 100141. N Y.
[32] P. Shannon, et al., Cytoscape: a software environment for integrated models of biomolecular interaction networks, Genome Res. 13 (11) (2003) 2498–2504.
[33] A. Mayakonda, et al., Maftools: efficient and comprehensive analysis of somatic variants in cancer, Genome Res. 28 (11) (2018) 1747–1756.
[34] P. Geeleher, N. Cox, R.S. Huang, Prrophetic: an r package for prediction of clinical chemotherapeutic response from tumor gene expression levels, PLOS One 9 (9) (2014), e107468.
[35] A. Subramanian, et al., A next generation connectivity map: L1000 platform and the first 1,000,000 profiles, Cell 171 (6) (2017) 1437–1452, e17.
[36] D. Bloniarz, et al., The lack of functional Dnmt2/Trdmt1 gene modulates cancer cell responses during drug-induced senescence, Aging 13 (12) (2021) 15833–15874. Albany NY.
[37] G. Betlej, et al., Deficiency of trdmt1 impairs exogenous RNA-based response and promotes retrotransposon activity during long-term culture of osteosarcoma cells, Toxicol. Vitro 80 (2022), 105323.
[38] X. Zhu, et al., ubiquitination-mediated degradation of TRDMT1 regulates homologous recombination and therapeutic response, NAR Cancer 3 (1) (2021) zcab010.
[39] M.Z. Zhang, et al., Renal medullary interstitial Cox-2 (cyclooxygenase-2) is essential in preventing salt-sensitive hypertension and maintaining renal inner medulla/papilla structural integrity, Hypertension, 72 (5) (2018) 1172–1179.
[40] X.R. Wu, Interstitial calcinosis in renal papillae of genetically engineered mouse models: relation to randall's plaques, Urolithiasis 43 (Suppl 1) (2015) 65–76.
[41] B. Chen, et al., Novel insights into biomarkers associated with renal cell carcinoma, Oncol. Lett. 16 (1) (2018) 83–90.
[42] Y. Chen, et al., Identifying the novel key genes in renal cell carcinoma by bioinformatics analysis and cell experiments, Cancer Cell Int. 20 (2020) 331.
[43] S. Basak, et al., Curcumin stimulates angiogenesis through Vegf And Expression Of Hla-G in first-trimester human placental trophoblasts, Cell Biol. Int. 44 (5) (2020) 1237–1251.
[44] Q. Zhang, et al., Overview of distinct 5-methylcytosine profiles of messenger RNA in human hepatocellular carcinoma and paired adjacent non-tumor tissues, J. Transl. Med. 18 (1) (2020) 245.
[45] J. Su, et al., Nsun2-Mediated Rna 5-methylcytosine promotes esophageal squamous cell carcinoma progression Via Lin28b-dependent Grb2 Mrna stabilization, Oncogene 40 (39) (2021) 5814–5828.
[46] M.R. Esposito, et al., Somatic mutations in specific and connected subpathways are associated with short neuroblastoma patients' survival and indicate proteins targetable at onset of disease, Int. J. Cancer 143 (10) (2018) 2525–2536.
[47] F. Safari, N.S Nejad, A. Aghaei Nejad, The inhibition Of Panc1 cancer cells invasion by hamscs secretome through suppression of tyrosine phosphorylation Of Sgk223 (At Y411 Site), C-Src (At Y416, Y530 Sites), Akt activity, And Jak1/Stat3 signaling, Med. Oncol. 39 (3) (2022) 28.
[48] J. Diring, et al., Rpel-family rhogaps link rac/cdc42 gtp loading To G-actin availability, Nat. Cell Biol. 21 (7) (2019) 845–855.
[49] Q. Chen, et al., A weighted gene co-expression network analysis-derived prognostic model for predicting prognosis and immune infiltration in gastric cancer, Front. Oncol. 11 (2021), 554779.
[50] T. Yi, et al., Regulatory network analysis of mutated genes based on multi-omics data reveals the exclusive features in tumor immune microenvironment between left-sided and right-sided colon cancer, Front. Oncol. 11 (2021), 685515.

[51] J. Gao, et al., Differential mutation detection capability through capture-based targeted sequencing in plasma samples in hepatocellular carcinoma, Front. Oncol. 11 (2021), 596789.
[52] S. Zhou, et al., Anaplastic Lymphoma Kinase (Alk) Rearrangement In Adult Renal Cell Carcinoma With Lung Metastasis: A Case Report And Literature Review, Transl. Androl. Urol. 9 (6) (2020) 2855–2861.
[53] M. Li, et al., Expression profiling and clinicopathological significance of dna methyltransferase 1, 3a and 3b in sporadic human renal cell carcinoma, Int J Clin Exp Pathol 7 (11) (2014) 7597–7609.
[54] J. Wang, et al., The Identification of a tumor infiltration Cd8+ T-cell gene signature that can potentially improve the prognosis and prediction of immunization responses in papillary renal cell carcinoma, Front. Oncol. 11 (2021), 757641.
[55] Y. Wang, et al., The interaction Of Ybx1 with G3bp1 promotes renal cell carcinoma cell metastasis via Ybx1/G3bp1-Spp1- Nf-kappab signaling axis, J. Exp. Clin. Cancer Res. 38 (1) (2019) 386.
[56] Y. Guan, et al., Dnmt3a and dnmt3b-decommissioned fetal enhancers are linked to kidney disease, J. Am. Soc. Nephrol. 31 (4) (2020) 765–782.
[57] Z.Z. Wang, et al., Alyref Associated With Immune Infiltration Is A Prognostic Biomarker In Hepatocellular Carcinoma, Transl Oncol 21 (2022), 101441.
[58] M. Klichinsky, et al., Human chimeric antigen receptor macrophages for cancer immunotherapy, Nat. Biotechnol. 38 (8) (2020) 947–953.
[59] H.C. Zhang, et al., Identification and validation in a novel quantification system of ferroptosis patterns for the prediction of prognosis and immunotherapy response in left- and right-sided colon cancer, Front. Immunol. 13 (2022), 855849.
[60] Z. Yang, et al., A Novel Defined Pyroptosis-Related Gene Signature For Predicting Prognosis And Treatment Of Glioma, Front. Oncol. 12 (2022), 717926.
[61] Z. Zhang, et al., An M6a-related lncrna signature predicts the prognosis of hepatocellular carcinoma, Front. Pharmacol. 13 (2022), 854851.
[62] H. Shi, et al., An efficient signature based on necroptosis-related genes for prognosis of patients with pancreatic cancer, Front. Genet. 13 (2022), 848747.
[63] S. Ren, et al., Crpmkb: a knowledge base of cancer risk prediction models for systematic comparison and personalized applications, Bioinformatics (2021).
[64] C. Wang, et al., Multi-omic profiling of plasma reveals molecular alterations in children with Covid-19, Theranostics 11 (16) (2021) 8008–8026.
[65] W. Ning, et al., Open resource of clinical data from patients with pneumonia for the prediction Of Covid-19 outcomes via deep learning, Nat. Biomed. Eng. 4 (12) (2020) 1197–1207.
[66] Y. Kataoka, et al., Integrated model for covid-19 diagnosis based on computed tomography artificial intelligence, and clinical features: a multicenter cohort study, Ann. Transl. Med. 10 (3) (2022) 130.
[67] D. Zhou, E.R. Gamazon, Integrative transcriptomic, evolutionary, and causal inference framework for region-level analysis: application to Covid-19, NPJ Genom. Med. 7 (1) (2022) 24.